Hindawi
Journal of Chemistry
Volume 2021, Article ID 9472008, 11 pages
https://doi.org/10.1155/2021/9472008

*Research Article*

# Facile One-Step Flame Synthesis of $La_{1-x}Sr_xMnO_3$ Nanoparticles for CO Catalytic Oxidation

**Hao Zhou, Qiwei Wu, and Boyang Qi**

*State Key Laboratory of Clean Energy Utilization, Institute for Thermal Power Engineering, Zhejiang University, Hangzhou 310027, China*

Correspondence should be addressed to Hao Zhou; zhouhao@cmee.zju.edu.cn

Received 24 July 2021; Accepted 3 September 2021; Published 24 September 2021

Academic Editor: Gang Feng



A large amount of CO as hazardous emission in the iron ore sintering process has caused severe harm to the environment and human health. To control the emission of CO more effectively, the preparation of highly efficient catalysts has attracted much attention. In this study, the $La_{1-x}Sr_xMnO_3$ ($0 \le x < 1$) perovskite catalysts with different $Sr^{2+}$ contents were prepared by the one-step flame synthesis method to treat CO pollutants in the iron and steel industry. The influence of $Sr^{2+}$ doping on the structure and activity of catalytic were characterized and analyzed. $La_{1-x}Sr_xMnO_3$ perovskite catalysts exhibit good perovskite phases and loose spherical structures. The specific surface areas are between 4.1 and 12.0 $m^2\ g^{-1}$. Combined with the results of $H_2$-TPR and $O_2$-TPD, the improvement of catalytic activity of $La_{1-x}Sr_xMnO_3$ perovskite can be attributed to the high concentration of active centers and oxygen vacancies. Significantly, the $La_{0.4}Sr_{0.6}MnO_3$ catalyst presented the best reducibility and high content of absorbed active oxygen species, leading to a superior CO oxidation catalytic activity and reaches 50% CO conversion at 134.9°C and 90% at 163.2°C, respectively. The effects of water vapor and $CO_2$ on the oxidation activity of $La_{1-x}Sr_xMnO_3$ perovskite was investigated. The flame-produced catalysts exhibit favorable catalytic stability and antisintering ability, achieving 100% CO conversion after fifth consecutive oxidation cycles.

## 1. Introduction

Carbon monoxide is a typical air pollutant, which is usually produced by the incomplete combustion of carbon-containing materials and hydrocarbons, such as coal, oil, and natural gas [1]. For example, a large amount of CO will also be produced in the start-up of motor vehicles, waste incineration, and industrial production [2]. Generally, in the iron ore sintering process, the CO concentration in the sintering flue gas is between 0.5% and 2% [3]. Meanwhile, the off-gas of industrial production usually contains relatively harmless compounds such as water vapor and carbon dioxide, which will cause some difficulties in removing CO [4]. Thus, it is necessary to explore a suitable method to control the emission of CO.

Among various CO removal methods, catalytic oxidation is considered to be the most effective way to eliminate this poisonous compound from the off-gas [5]. Noble metal catalysts (Ru, Pt, and Au) exhibit high catalytic activity and have been widely researched in CO oxidation. However, they are susceptible to sintering, expensive, and the activity decreases with the increased reaction time [6, 7]. Compared with noble metal catalysts, the perovskite-type catalysts with $ABO_3$ structure have excellent catalytic activity, high thermal stability, and good structural stability, regarded as a promising candidate catalyst [8]. In addition, the partial substitution of A/B sites can change the cation valence of perovskite to affect the catalytic activity. According to previous research reports, lanthanum-based perovskite, such as $La_{1-x}Sr_xMnO_3$, has good catalytic activity and is suitable for CO oxidation. Frozandeh-Mehr et al. [9] studied the CO oxidation activity of $La_{1-x}Sr_xMnO_3$ ($0 \le x < 0.4$). Sr-doping does not affect the single-phase perovskite-type formation and can decrease the CO catalytic oxidation temperature. Teng et al. [10] synthesized the perovskite of $La_{0.5}Sr_{0.5}MnO_3$ by hydrothermal and citrate routes for CO

oxidation, in which the complete oxidation temperature of CO was below 220°C. Peng et al. [11] prepared $La_{1-x}Sr_xMnO_3$ ($0 \le x \le 0.3$) with metal foam (MF) as composite catalysts for CO oxidation. They found $Sr^{2+}$ doped could significantly improve the catalyst activity. Hence, Sr-doped perovskite was used for CO oxidation in this work.

Flame synthesis is a fast, economical, and one-step thermal spraying technology. It has attracted much attention due to its rapid preparation with a simplified collection process. The synthesis rate of nanoparticles can reach 30–100 g/h [12]. In the flame synthesis process, the combustible precursor solution with a certain concentration of metal ions compounds was ignited by a high-temperature flame and the products formed in a short time. Then, the nanoparticles are filtered and collected [13, 14]. Nanoparticles prepared by the flame synthesis method have been widely used as functional ceramic powders. Abe and Laine [15] prepared perovskite-type nanoparticles $La_2TiO_7$ by the flame spray pyrolysis method, and the catalysis had superior photocatalytic activity. And it is very conducive to the preparation of nanoparticle perovskite catalysts with specific morphology and precise chemical composition. Kim et al. [16] synthesized $La_{0.2}Sr_{0.8}Co_{1-x}Fe_xO_{3-\delta}$ and $Ba_{0.5}Sr_{0.5}Co_{1-x}Fe_xO_{3-\delta}$ nanoparticles perovskites by the flame synthesis, and the results showed that oxygen evolution activity was improved. However, most of the currently reported high-efficiency perovskite catalysts for CO oxidation are synthesized in traditional ways, such as coprecipitation [17], hydrothermal [18], and sol-gel synthesis [19]. And the obtained perovskite catalysts need to be calcined at high temperatures, leading to complex operations and low productivity. Therefore, it is necessary to develop an alternative method for the one-step synthesis of perovskite catalysts for CO oxidation with desired physical and chemical properties.

This study synthesized a series of $La_{1-x}Sr_xMnO_3$ ($0 \le x < 1$) perovskites catalysts with different $Sr^{2+}$ contents by a one-step flame synthesis method for CO oxidation. The performance evaluation and physicochemical properties of flame-produced nanoparticles were comprehensively analyzed. The effects of Sr-doping on the properties of catalysts were revealed.

## 2. Experimental Section

*2.1. Perovskite Catalysts Preparation.* $La_{1-x}Sr_xMnO_3$ ($0 \le x < 1$) perovskite catalysts were prepared by the flame synthesis method, as shown in Figure 1. For starting, an appropriate proportion of La $(NO_3)_3{\cdot}6H_2O$ (Macklin, >99.9%), Mn $(NO_3)_3{\cdot}4H_2O$ (Macklin, >99.9%), and Sr $(NO_3)_2$ (Macklin, >99.5%) were dissolved in the anhydrous ethanol to obtain a total metal ion concentration of 0.2 mol/L. Meanwhile, the $Sr^{2+}/La^{3+}$ molar ratio was controlled as 0, 1/4, 2/3, 3/2, and 4, respectively. Then, the corresponding solution was controlled by a Microflow syringe pump at a constant flow rate of 1.2 mL/min via a central nozzle of the McKenna flame burner. Simultaneously, 0.75 L/min of atomized air was injected as dispersion gas to form a stable precursor spray. The atomized precursor was ignited by the supporting flat flame of the burner (2 L/min, $CH_4$+20 L/min, air). The precursor spray was heated, oxidized, and sintered due to the energy released during the reaction. Finally, the nanoparticles were collected on the glass fiber filters with the help of negative pressure formed by the vacuum pump.

*2.2. Catalyst Characterization.* The crystallinity and phase purity of perovskite catalysts are measured by the X-ray diffractometer (XRD). The diffraction patterns were analyzed in a continuous scan mode with a range of 20°–80° and 0.02°per second sampling interval. The morphology of the synthesized powder was studied by field-emission scanning electron microscopy (FE-SEM). And the bulk composition of perovskite samples was determined by the energy-dispersive spectroscopy (EDS) plane scanning method. And the semiquantitative chemical composition characterization was measured with an atomic and mass percentage at three zones for each sample. Nitrogen physisorption isotherms determined the textural properties of the catalysts at −196°C on the Quantachrome AUTOSORB-1C analyzer. The specific surface area (SSA) of the catalyst was calculated by the Brunauer–Emmett–Teller (BET) method. And $H_2$ temperature-programmed reduction ($H_2$-TPR) was applied to the samples on an automatic chemisorption machine (BelCata II, Japan). A thermal conductivity detector (TCD) was used to record the signal and calculate the total $H_2$ consumption. The desorption temperature and intensity of different oxygen species were studied by $O_2$ temperature-programmed desorption ($O_2$-TPD). And the desorption amount of $O_2$ during the TPD process was calculated.

*2.3. Catalytic Activity.* The catalytic activity of perovskite samples for CO oxidation was conducted in a quartz tube-fixed bed reactor, and the reaction temperature was controlled by a programmed electrical pipe furnace. Figure 2 shows a schematic diagram of the CO catalytic oxidation experiment, and the test conditions are given in Table 1. Prior to the reaction, 1 g of the sample was packed in the quartz tube reactor. The reaction gas (1.0 vol% CO, 10.0 vol% $O_2$, and balanced with Ar) was introduced with regulation by the mass flow controllers, and the total flow rate was 1.5 L/min. In the mixed gas test, 10.0 vol% $CO_2$ and 5.0 vol% water vapor were injected into the reactor with the same stream of $CO/O_2$ balance Ar. The heating stage was performed from room temperature up to 300°C at a rate of 6°C/min. The CO concentration was continuously measured by a flue gas analyzer (Testo 350). Five consecutive catalytic oxidation experiments were carried out to explore the long-term stability of the perovskite catalysts. And the CO conversion was calculated after steady-state by the following equation.

$$CO_{Conv}\% = \frac{(CO_{in} - CO_{out})}{CO_{in}} \times 100\%, \quad (1)$$

where $CO_{Conv}$ is the CO conversion efficiency, and $CO_{in}$ and $CO_{out}$ represent the CO concentration of inlet and outlet.

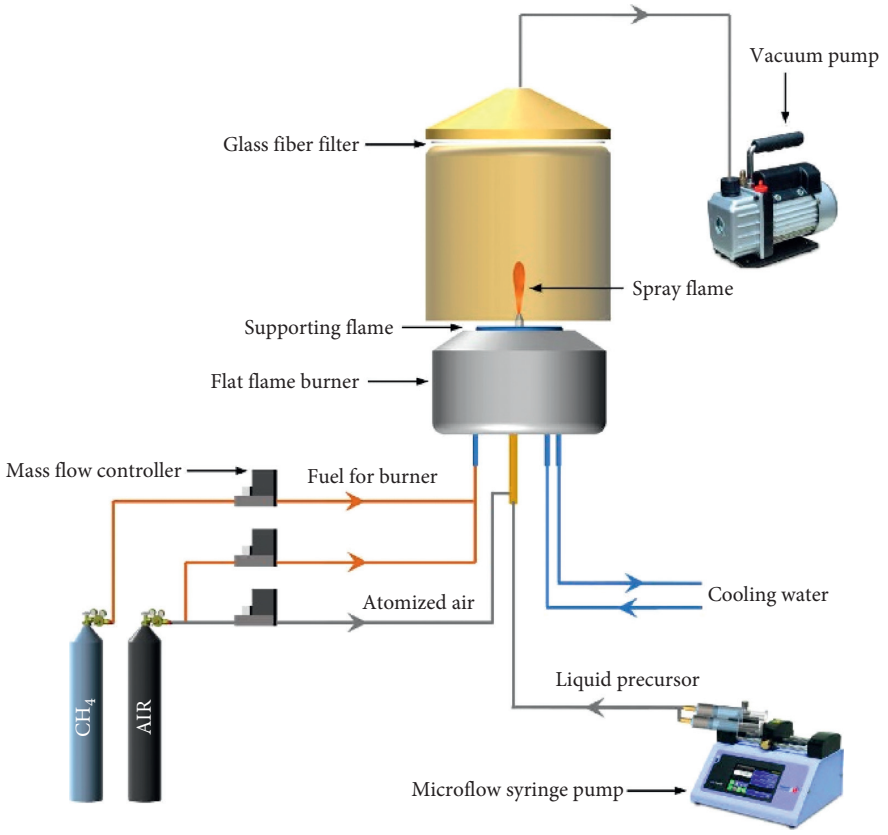


Figure 1: Scheme of the flame synthesis system.

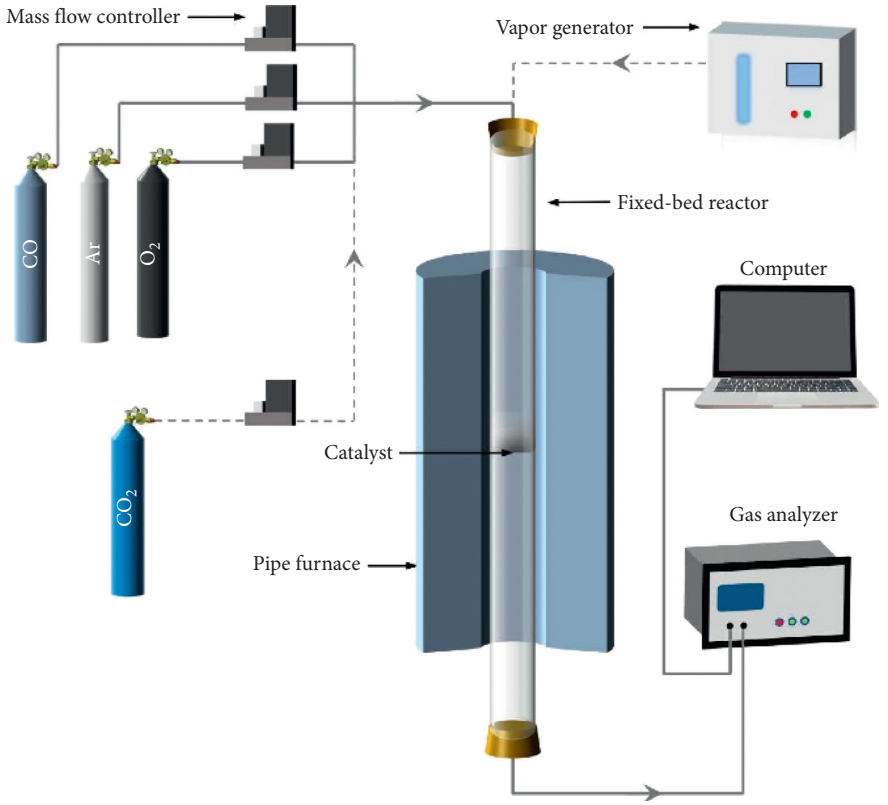


Figure 2: Fixed bed system for catalytic oxidation of CO with perovskite catalysts.

Table 1: Experimental conditions for the catalyst performance test.

| Test | CO vol (%) | $O_2$ vol (%) | Ar vol (%) | $CO_2$ vol% | Water vapor vol% |
|---|---|---|---|---|---|
| Case 1 | 1 | 10 | 89 | 0 | 0 |
| Case 2 | 1 | 10 | 74 | 10% | 5% |

## 3. Results and Discussion

*3.1. Structural Characterization.* Figure 3 shows the XRD patterns of $La_{1-x}Sr_xMnO_3$ ($0 \le x < 1$) perovskite catalyst. As shown in Figure 3(a), when $x = 0$, the characteristic peaks at $2\theta$ angles are 19.3°, 32.3°, 40.1°, 47.1°, 53.4°, 57.6°, 67.6°, and 77.5°, and all diffraction peaks are well indexed to that of $LaMnO_3$ perovskite (PDF-ICDD 75–0440). However, excessive $Sr^{2+}$ doping leads to the appearance of $Mn_2O_3$ and $La_2O_3$ phases, which should be attributed to the lattice distortion with $Sr^{2+}$ doping during the synthesis process, and the solubility of cations is limited [20]. The intensity and position of the main diffraction peak of five catalysts do not change significantly and keep in the perovskite phase structure, which is essential for the catalytic reaction [5]. As shown in Figure 3(b), the patterns of the $La_{0.8}Sr_{0.2}MnO_3$ sample have small splitting of the main peak at 32.5°, which indicates the second crystal form of perovskites. And it may be related to the synthesis method and preparation conditions of perovskite [9]. Furthermore, it is observed that the diffraction peaks for $x = 0.2$–$0.8$ are shifted toward a higher angle orientation over those substituted catalysts in comparison with $LaMnO_3$. The partial substitution of $La^{3+}$ by $Sr^{2+}$ will lead to $Mn^{3+}$ ($r = 0.58$ Å) transfer into smaller $Mn^{4+}$ ($r = 0.53$ Å), resulting in lattice shrinkage [21, 22]. And the gradual shifts toward high-angle orientation could be induced by the decrease in interplanar distance after strontium substitution [23]. A similar phenomenon regarding the diffraction angle shift was previously reported by Li et al. [21]. And the specific surface area (SSA) of $La_{1-x}Sr_xMnO_3$ is given in Table 2. It is obvious that $Sr^{2+}$ substitution improved the surface area to some extent, and the SSA of $La_{1-x}Sr_xMnO_3$ is 4.1, 6.2, 8.4, 10.2, and 12.0 $m^2\ g^{-1}$, corresponding to $x = 0$, 0.2, 0.4, 0.6, and 0.8, respectively. The maximum specific surface area is found on $La_{0.2}Sr_{0.8}MnO_3$ (12.0 $m^2\ g^{-1}$). Moreover, the larger specific surface area is considered an effective way to improve the catalytic activity.

Figure 4 shows the FE-SEM images of $La_{1-x}Sr_xMnO_3$ ($0 \le x < 1$). The flame-produced perovskite nanoparticles show loose and porous spherical structures with a diameter of 300–500 nm. As seen from the images, the particle size tends to decrease, and the porosity increases gradually, consistent with the results of the specific surface area. However, some small particles begin to appear on the surface of the catalysts with the addition of $Sr^{2+}$. Combined with XRD results, it could be ascribed to the phase segregation caused by excessive $Sr^{2+}$ during the flame preparation process [9]. The EDS analysis is also performed, and the distribution of different elements in the catalyst is further studied. In the case of $La_{0.4}Sr_{0.6}MnO_3$, as shown in Figure 5, the La, Sr, Mn, and O atoms are homogeneously and finely dispersed in the sample. And the atomic ratios of catalysts are presented in Table 3. The atomic ratio of La and Mn were similar for $LaMnO_3$, 50.44% and 49.56%, respectively. The theoretical deviation (La + Sr)/Mn in the perovskite samples prepared by the flame synthesis method is in good accordance with the nominal ones.

$H_2$ temperature-programmed reduction ($H_2$-TPR) experiments were used to characterize the reduction properties and determine the reaction temperature of the samples. Figure 6 shows that all the samples have similar reduction peaks with two main reduction regions between 150°C and 850°C, which can be divided into a low-temperature region (below 500°C) and a high-temperature region (above 500°C) [22]. With regard to low-temperature regions, the TPR signal begins to appear at 150–200°C, which is related to the reduction of adsorbed oxygen species on the surface [24]. Based on the previous reports, even stoichiometric $LaMnO_3$ perovskite would exhibit an $Mn^{3+}/Mn^{4+}$ mixed oxidation state, balanced by excess oxygen in the lattice [5]. Hence, the peak around 300°C can be attributed to removing the nonstoichiometric excess oxygen contained in the perovskite lattice. For Sr-substituted $LaMnO_3$ catalysts, the reduction peak at 450°C can be attributable to the reduction of $Mn^{4+}$ to $Mn^{3+}$. The reaction of the process can be written as equations (2) and (3). Compared with pure $LaMnO_3$ in Figure 6, the peak signal of $Sr^{2+}$-doped samples increase and move to low temperature. It indicates that the substitution of $Sr^{2+}$ facilitated the oxidation capacity of catalysts in the low-temperature region, which is significant to improving the catalyst's activity in CO catalytic oxidation.

$$La_{1-x}Sr_xMn_{1-x}^{3+}Mn_x^{4+}O_{3+\delta} + \delta H_2 \longrightarrow La_{1-x}Sr_xMn_{1-x}^{3+}Mn_x^{4+}O_3 + \delta H_2O \quad (2)$$

$$La_{1-x}Sr_xMn_{1-x}^{3+}Mn_x^{4+}O_3 + \frac{1}{2}xH_2 \longrightarrow La_{1-x}Sr_xMn^{3+}O_{3-x/2} + \frac{1}{2}xH_2O \quad (3)$$

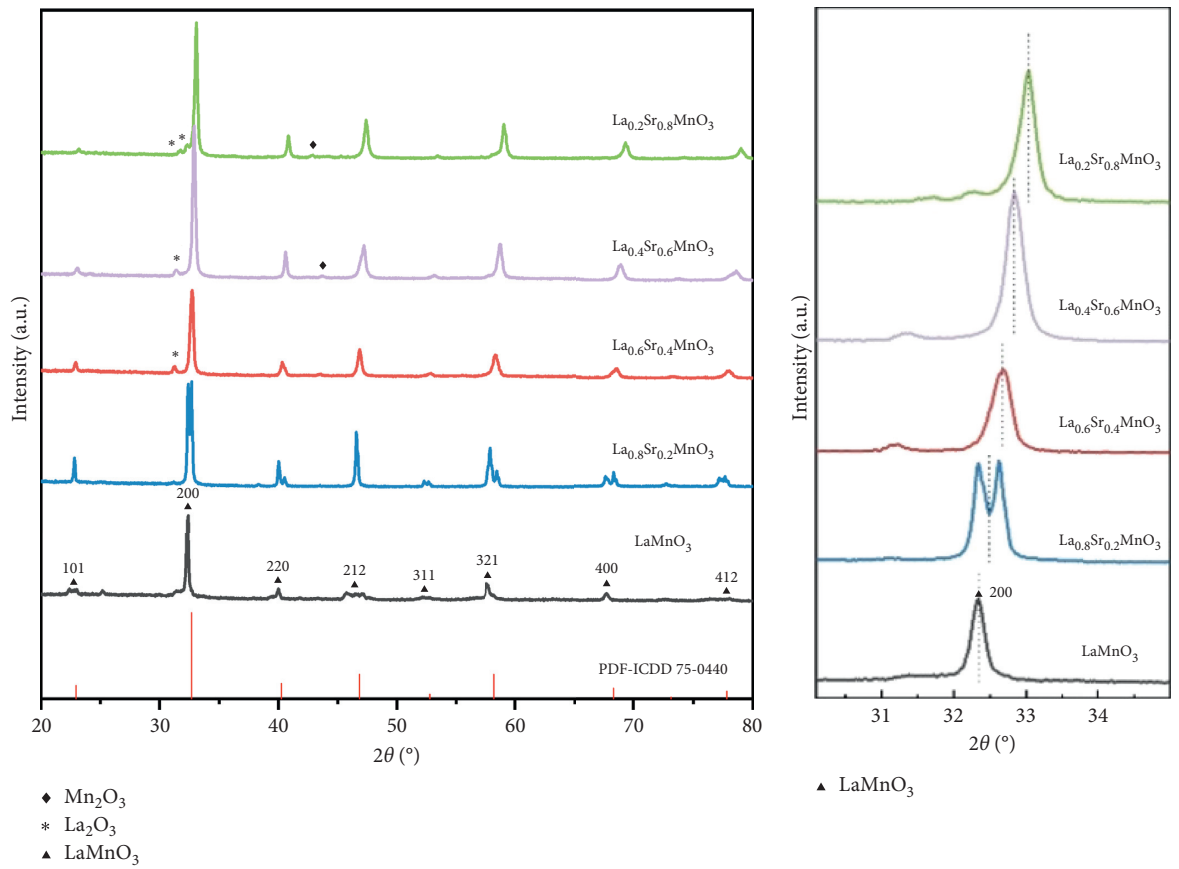


Figure 3: XRD patterns of (a) $La_{1-x}Sr_xMnO_3$ ($0 \le x < 1$) and (b) the main peak (200) crystal plane ($2\theta = 31^\circ$–$34^\circ$).

Table 2: Specific surface area of $La_{1-x}Sr_xMnO_3$ ($0 \le x < 1$) catalysts.

| Catalysts | SSA[a] ($m^2\ g^{-1}$) |
|---|---|
| $LaMnO_3$ | 4.1 |
| $La_{0.8}Sr_{0.2}MnO_3$ | 6.2 |
| $La_{0.6}Sr_{0.4}MnO_3$ | 8.4 |
| $La_{0.4}Sr_{0.6}MnO_3$ | 10.2 |
| $La_{0.2}Sr_{0.8}MnO_3$ | 12.0 |

[a]Determined by $N_2$ adsorption (BET method).

Another intense reduction peak at the high-temperature region is observed, ascribed to the reduction of $Mn^{3+}$ into $Mn^{2+}$. The reaction of the process is written in the following equation.

$$La_{1-x}Sr_xMn^{3+}O_{3-x/2} + \frac{1}{2}H_2 \longrightarrow \frac{1}{2}(1-x)La_2O_3 + xSrO + MnO + \frac{1}{2}H_2O \quad (4)$$

The total $H_2$ consumption of $La_{1-x}Sr_xMnO_3$ ($0 \le x < 1$) catalysts is calculated by the quantitative analysis and illustrated in Table 4. Noticeably, as the $Sr^{2+}$ substitution increases from 0 to 0.8, the total $H_2$ consumption of $La_{1-x}Sr_xMnO_3$ is 1.36 mmol $g^{-1}$, 1.97 mmol $g^{-1}$, 2.10 mmol $g^{-1}$, 2.91 mmol $g^{-1}$, and 2.85 mmol $g^{-1}$, respectively. $La_{0.6}Sr_{0.4}MnO_3$ has the highest $H_2$ consumption among all the catalysts, in which the reduction activity is presumed to be the best.

The profiles of $O_2$-TPD measurements are shown in Figure 7. Compared with other samples, the $O_2$ desorption signal of $LaMnO_3$ is relatively weak. There are three major regions in the TPD profile that begin to appear with the increase of $Sr^{2+}$ doping content and are denoted as $O_I$, $O_{II}$, and $O_{III}$.

The $O_I$ region below 350°C is ascribed to the chemisorbed oxygen on the surface of the catalyst [23]. This active oxygen is essential for catalytic activity, which can directly participate in the CO oxidation reaction due to the weak adsorption relationship between chemisorbed oxygen and the perovskite surface. In the $O_{II}$ region, there is a main peak between 350°C and 550°C. This signal is attributed to the

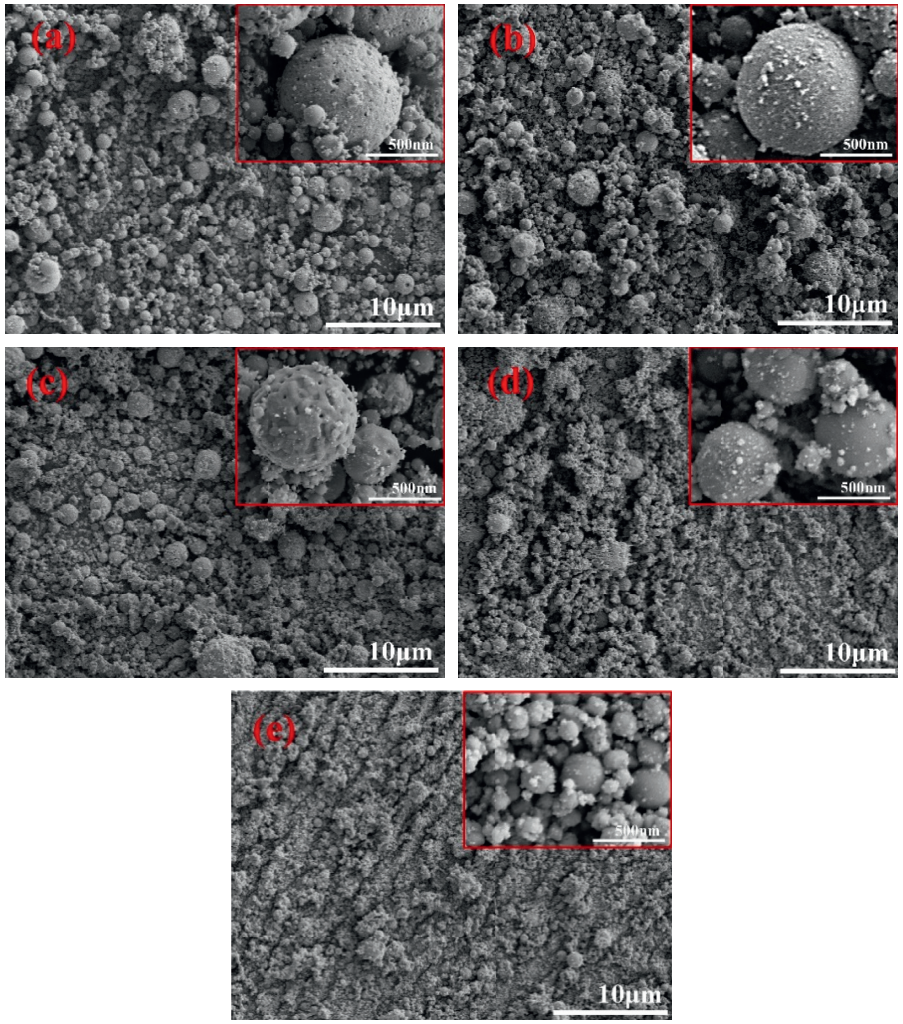


Figure 4: SEM images of $La_{1-x}Sr_xMnO_3$ with $x = 0$ (a), 0.2 (b), 0.4 (c), 0.6 (d), and 0.8 (e).

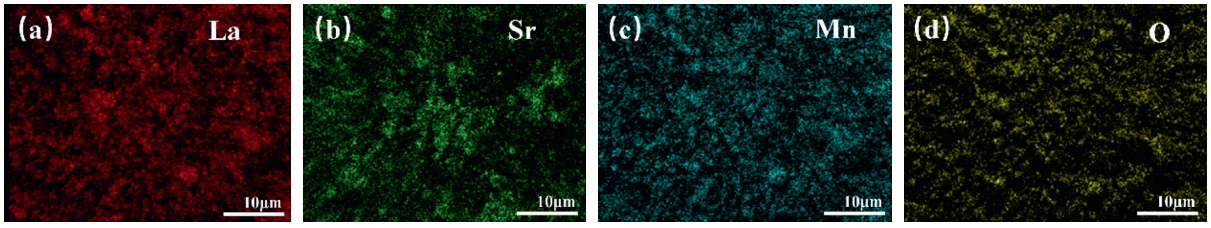


Figure 5: EDS mapping images of $La_{0.4}Sr_{0.6}MnO_3$ catalysts (a) La, (b) Sr, (c) Mn, and (d) O.

removal of mobile interface oxygen, which can take part in the catalytic oxidation reaction by migrating from the interior of the lattice to the surface. Furthermore, it can be found that the signal intensity of $La_{0.4}Sr_{0.6}MnO_3$ and $La_{0.2}Sr_{0.8}MnO_3$ was strengthened in comparison with $LaMnO_3$. The TCD signals in the $O_{III}$ region with a temperature above 550°C are mainly related to the bulk lattice oxygen and could reflect the lattice oxygen mobility [25]. Normally, the desorption capacity is related to the properties of B site metal ions in the perovskite structure [26]. At the low temperature, the oxygen in $O_I$ region was removed, and then, $O_{II}$-oxygen was released with the increase of temperature, leading to the reduction of Mn ions and the generation of surface oxygen vacancies. After that, $O_{III}$-oxygen diffuses from the bulk to the catalyst surface and desorbs [27]. Moreover, the desorption signal of $La_{1-x}Sr_xMnO_3$ ($0 \le x < 1$) increases gradually and tends to move to the low-temperature region, suggesting that $Sr^{2+}$ has a positive effect on the surface oxygen capacity and oxygen mobility. According to the quantitative results of $O_2$-TPD in Table 4, it can be seen that Sr-doped perovskite catalysts exhibited higher desorption amounts of oxygen in

Table 3: EDS results of $La_{1-x}Sr_xMnO_3$ ($0 \le x < 1$).

| Catalysts | | Atomic ratio (%) | | | |
|---|---|---|---|---|---|
| | | La | Sr | Mn | (La + Sr)/Mn |
| $LaMnO_3$ | Nominal | 50.00 | 0.00 | 50.00 | 1.00 |
| | SEM-EDS | 50.44 | 0.00 | 49.56 | 1.02 |
| $La_{0.8}Sr_{0.2}MnO_3$ | Nominal | 40.00 | 10.00 | 50.00 | 1.00 |
| | SEM-EDS | 41.91 | 8.53 | 49.57 | 1.02 |
| $La_{0.6}Sr_{0.4}MnO_3$ | Nominal | 30.00 | 20.00 | 50.00 | 1.00 |
| | SEM-EDS | 31.12 | 18.79 | 50.10 | 0.99 |
| $La_{0.4}Sr_{0.6}MnO_3$ | Nominal | 20.00 | 30.00 | 50.00 | 1.00 |
| | SEM-EDS | 20.05 | 31.75 | 48.19 | 1.07 |
| $La_{0.2}Sr_{0.8}MnO_3$ | Nominal | 10.00 | 40.00 | 50.00 | 1.00 |
| | SEM-EDS | 10.67 | 39.35 | 49.98 | 1.00 |

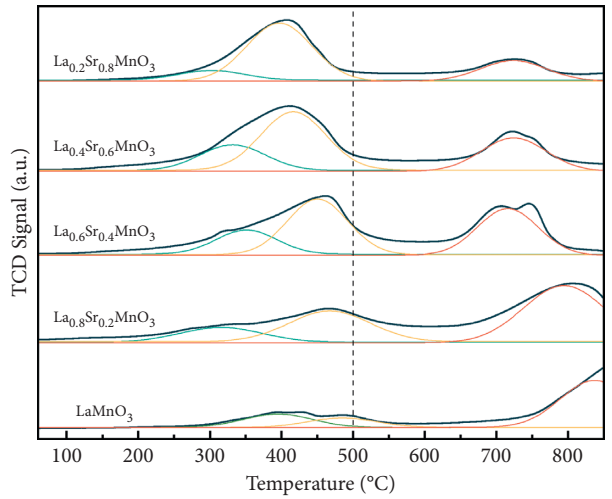


Figure 6: $H_2$-TPR profiles of $La_{1-x}Sr_xMnO_3$ ($0 \le x < 1$).

Table 4: Quantitative results of $H_2$-TPR and $O_2$-TPD profiles.

| Catalysts | $H_2$ consumption (mmol $g^{-1}$) | | | $O_2$ desorption ($\mu$mol $g^{-1}$) | | |
|---|---|---|---|---|---|---|
| | L. T. R[a] | H. T. R[b] | Total | $O_I$ | $O_{II}$ | $O_{III}$ |
| $LaMnO_3$ | 0.38 | 0.98 | 1.36 | 43 | 52 | 117 |
| $La_{0.8}Sr_{0.2}MnO_3$ | 0.65 | 1.32 | 1.97 | 75 | 66 | 125 |
| $La_{0.6}Sr_{0.4}MnO_3$ | 1.12 | 0.98 | 2.10 | 94 | 78 | 159 |
| $La_{0.4}Sr_{0.6}MnO_3$ | 1.96 | 0.95 | 2.91 | 117 | 121 | 217 |
| $La_{0.2}Sr_{0.8}MnO_3$ | 1.86 | 0.99 | 2.85 | 125 | 177 | 396 |

[a]Low-temperature reduction region. [b]High-temperature reduction region.

three regions than the $LaMnO_3$ sample, indicating that they have superior oxygen storage capacity and oxygen migration capacity. Furthermore, the $La_{0.2}Sr_{0.8}MnO_3$ sample presents the highest total desorption amount (698 $\mu$mol g − 1), beneficially due to the larger specific surface area and the positive role of Sr dopant in oxygen mobility elevation [28].

*3.2. Catalytic Activity of Perovskite.* The CO catalytic activity of $La_{1-x}Sr_xMnO_3$ ($0 \le x < 1$) was evaluated, as shown in Figure 8(a). All the catalysts presented good catalytic activity, and the CO conversion presents an obvious S-shape curve during the heating process, which can reach 90% at 170–210°C and then to 100% quickly. And the temperature of full CO conversion is below 250°C. Moreover, $La_{0.4}Sr_{0.6}MnO_3$ exhibits the optimum CO catalytic activity with the lowest T50 and T90 at 134.9°C and 163.2°C, respectively. The results show that the substitution of $Sr^{2+}$ is beneficial to the CO oxidation activity of perovskite catalyst. And the improvement of $La_{1-x}Sr_xMnO_3$ perovskite catalysts in CO catalytic oxidation can be attributed to the synergistic effect between the larger specific surface area and the high number of active sites of catalysts [11]. Furthermore, combined with the results of $H_2$-TPR and $O_2$-TPD, the

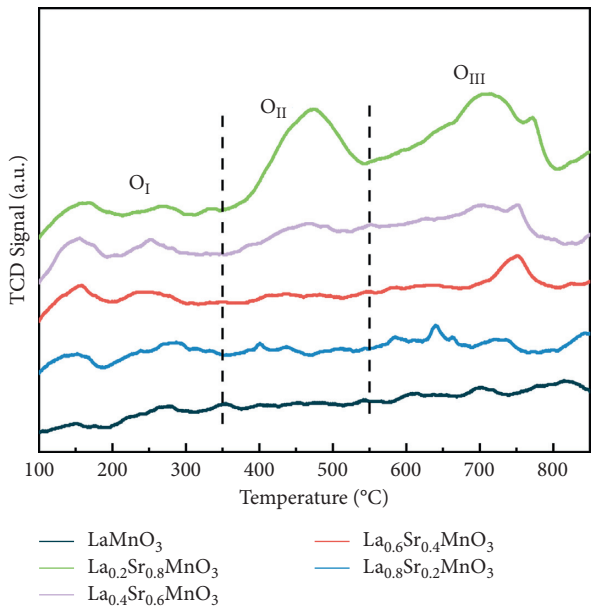


Figure 7: $O_2$-TPD profiles of $La_{1-x}Sr_xMnO_3$ ($0 \le x < 1$).

substitution of $Sr^{2+}$ promoted the decrease of reduction temperature and the improvement of oxygen migration activity. However, the CO catalytic performance of $La_{0.2}Sr_{0.8}MnO_3$ is slightly weaker than that of $La_{0.4}Sr_{0.6}MnO_3$. It may be due to the phase segregation of $Mn_2O_3$ and $La_2O_3$ with the excessive $Sr^{2+}$ doping amount, which occupies the effective area of active sites on the catalyst surface. And the destruction of perovskite structure will lead to degradation of CO catalytic performance.

In the off-gas of the iron ore sintering industry, water vapor and carbon dioxide usually coexist with CO. They will adsorb on the catalyst surface, resulting in the deactivation of the catalyst. Herein, the effect of water vapor and carbon dioxide on catalytic activity is investigated. Figure 8(b) shows that the performance of five catalysts decreased slightly in the range of 5%–15%, and the pure $LaMnO_3$ achieves T90 at around 210°C. In comparison, $La_{0.4}Sr_{0.6}MnO_3$ has the highest catalytic activity, and T50 and T90 are 153.1°C and 181.5°C, respectively. Zhang et al. [23] reported Ni partial substitution of $LaMnO_3$ perovskite under a wet condition and found that the degradation of catalyst performance may be the competitive adsorption of water vapor with $O_2$. In addition, the O–OH species formed on the surface adsorption competition will limit the access of the reactant molecules to the sample surface, inhibiting the adsorption of CO on the $Mn^{4+}$ active site. In order to study the intrinsic activity of $La_{1-x}Sr_xMnO_3$ catalyst, the ratio of the CO oxidation rate to active oxygen density was measured by isothermal reaction at 120°C. And the TOF value was obtained, as given in Table 5. Compared with pure $LaMnO_3$ catalyst, Sr-doped materials possessed a higher reaction rate, which suggested that the introduction of Sr ions promotes the adsorption of $O_2$ and the mass transfer of reactants and products on the perovskite surface [29, 30]. $La_{0.4}Sr_{0.6}MnO_3$ shows the highest TOF value, which is $2.08 \times 10^{-3}$ $s^{-1}$. However, when $x = 0.8$, the TOF value of $La_{0.2}Sr_{0.8}MnO_3$ sample decreased, which means that the catalytic activity did not further increase and is consistent with the experimental results of CO catalytic oxidation.

The consecutive oxidation experiments of $La_{1-x}Sr_xMnO_3$ were carried out to explore the stability of catalytic performance. And the results are given in Tables 6 and 7. After five times consecutive oxidations, all samples can achieve full CO conversion, and the degradation was less than 15%. For comparison, $La_{0.4}Sr_{0.6}MnO_3$ shows superior catalytic activity, which achieved 90% CO conversion at 176.9°C and 194.6°C, respectively. And the decrease of catalytic activity may be due to the consumption of surface chemisorbed oxygen and the reduction of some active sites by CO in the reaction [31]. The XRD patterns of the catalyst after the consecutive oxidation test are shown in Figure 9. Compared with the XRD characterization before and after the reaction, the intensity and position of diffraction peaks do not change significantly after the cyclic test, which demonstrated that the perovskite structure of samples is retained during the consecutive oxidation test. On the other side, the rapid sintering of precursor sprays in high-temperature flame (>1000°C) increased the dispersion and sintering resistance of Mn active components in perovskite catalysts [32]. Ding et al. [28] also reported the preparation of metal oxide-supported single-atom Pt catalysts with high thermal stability by flame spray pyrolysis. Compared with the conventional impregnation method, the flame spray pyrolysis is more conducive to forming the tetragonal-monoclinic phase of $ZrO_2$, thus improving the sintering resistance at high temperature. Hence, the above results indicate that the flame synthesis method is suitable for preparing perovskite catalysts with superior long-term stability and high CO catalytic activity.

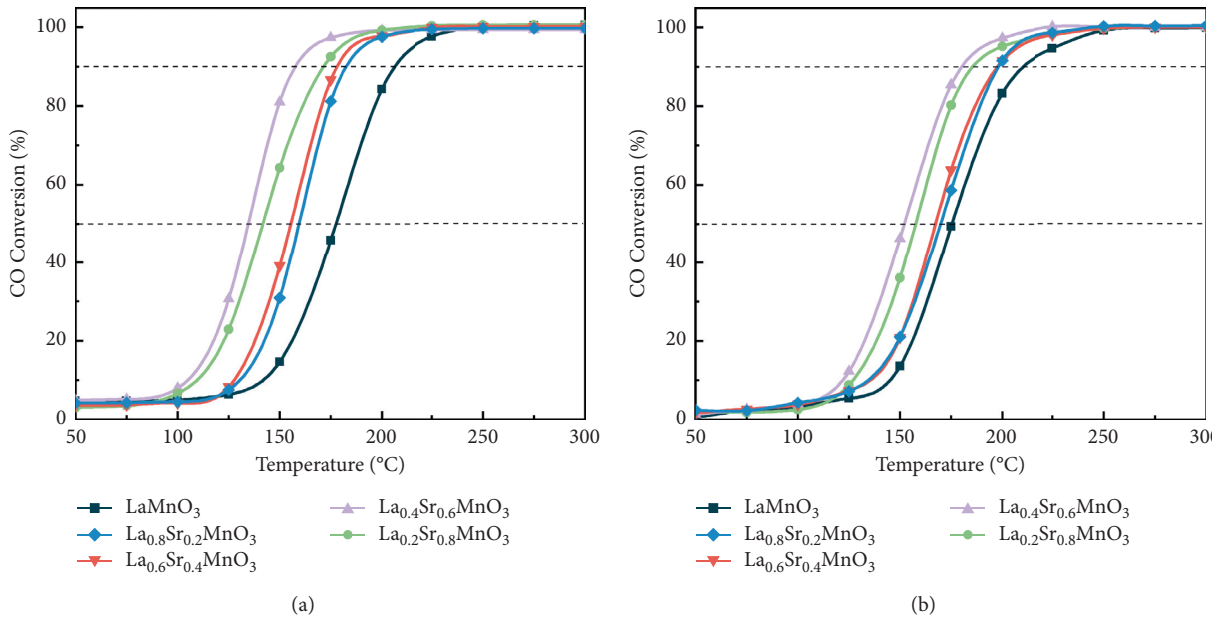


Figure 8: Catalytic performance for CO oxidation of $La_{1-x}Sr_xMnO_3$ ($0 \le x < 1$) under two conditions. (a) Case 1 of 1.0 vol% CO, 10.0 vol% $O_2$, and Ar balance. (b) Case 2 of adding 5.0 vol% water vapor and 10.0 vol% $CO_2$.

Table 5: Reaction performance of $La_{1-x}Sr_xMnO_3$ catalysts.

| Catalysts | Reaction rate ($\mu$mol $g^{-1}$ $s^{-1}$) | TOF ($10^{-3}$ $s^{-1}$) |
|---|---|---|
| $LaMnO_3$ | 0.075 | 1.74 |
| $La_{0.8}Sr_{0.2}MnO_3$ | 0.134 | 1.79 |
| $La_{0.6}Sr_{0.4}MnO_3$ | 0.173 | 1.84 |
| $La_{0.4}Sr_{0.6}MnO_3$ | 0.243 | 2.08 |
| $La_{0.2}Sr_{0.8}MnO_3$ | 0.236 | 1.89 |

Table 6: Temperature values of 50% and 90% conversion in CO catalytic oxidation.

| Case1 catalytic cycles | $LaMnO_3$ | | $La_{0.8}Sr_{0.2}MnO_3$ | | $La_{0.6}Sr_{0.4}MnO_3$ | | $La_{0.4}Sr_{0.6}MnO_3$ | | $La_{0.2}Sr_{0.8}MnO_3$ | |
|---|---|---|---|---|---|---|---|---|---|---|
| | T50 | T90 | T50 | T90 | T50 | T90 | T50 | T90 | T50 | T90 |
| 1st | 170.6 | 201.8 | 161.5 | 185.2 | 153.3 | 182.1 | 134.9 | 163.2 | 140.4 | 173.6 |
| 2nd | 178.7 | 205.5 | 161.6 | 189.6 | 159.4 | 186.2 | 135.3 | 165.8 | 147.7 | 173.9 |
| 3rd | 178.3 | 208.1 | 162.8 | 194.4 | 162.7 | 191.7 | 137.9 | 169.2 | 151.2 | 174.3 |
| 4th | 174.6 | 207.8 | 162.1 | 190.9 | 158.1 | 187.6 | 138.4 | 164.7 | 151.4 | 177.6 |
| 5th | 178.1 | 210.2 | 163.6 | 195.3 | 161.3 | 189.1 | 143.6 | 176.9 | 151.1 | 179.5 |

Table 7: Temperature values of 50% and 90% conversion in CO catalytic oxidation of mixture atmosphere.

| Case2 catalytic cycles | $LaMnO_3$ | | $La_{0.8}Sr_{0.2}MnO_3$ | | $La_{0.6}Sr_{0.4}MnO_3$ | | $La_{0.4}Sr_{0.6}MnO_3$ | | $La_{0.2}Sr_{0.8}MnO_3$ | |
|---|---|---|---|---|---|---|---|---|---|---|
| | T50 | T90 | T50 | T90 | T50 | T90 | T50 | T90 | T50 | T90 |
| 1st | 181.8 | 209.2 | 167.1 | 197.2 | 167.7 | 196.6 | 153.1 | 181.5 | 154.3 | 188.7 |
| 2nd | 175.9 | 212.1 | 172.8 | 203 | 164.7 | 196.7 | 152.8 | 182.9 | 158.3 | 192.4 |
| 3rd | 181.3 | 220.3 | 171.5 | 203.8 | 174.2 | 206.9 | 154.6 | 188.4 | 157.1 | 193.8 |
| 4th | 174.2 | 214.8 | 168.9 | 201.4 | 169.9 | 203.9 | 154.9 | 185.6 | 156.1 | 194.3 |
| 5th | 185.2 | 223.8 | 170.5 | 201.6 | 173.5 | 206.6 | 164.2 | 194.6 | 162.3 | 199.6 |

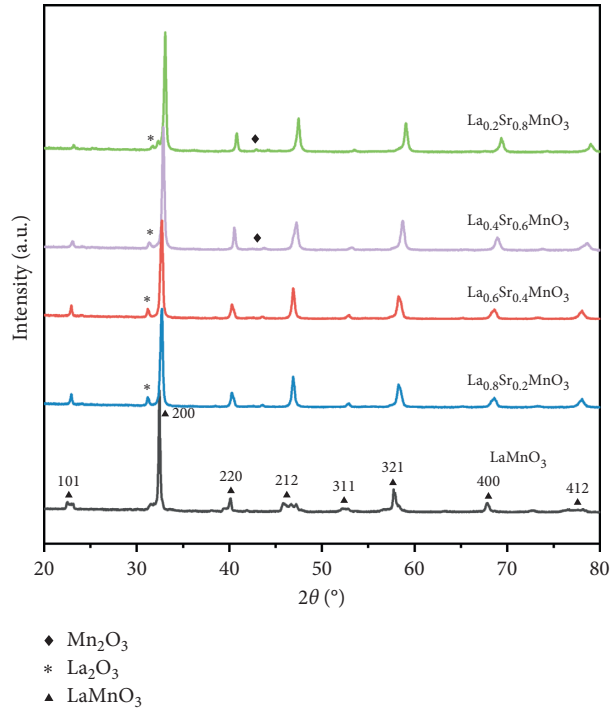


Figure 9: XRD patterns of $La_{1-x}Sr_xMnO_3$ after activity tests.

## 4. Conclusion

In summary, $La_{1-x}Sr_xMnO_3$ ($x = 0$, 0.2, 0.4, 0.6, 0.8) perovskite catalyst was successfully prepared by the one-step flame synthesis method for CO catalytic oxidation. The unique synthesis route conducts a fast and efficient production, leading to good perovskite phases and loose spherical structures. The specific surface area increases from 4.1 to 12.0 $m^2\ g^{-1}$ with $Sr^{2+}$ doping. According to the $H_2$-TPR and $O_2$-TPD test results, the $Sr^{2+}$ partial substitution promotes the number of active sites and oxygen vacancies, improving the redox activity. The catalyst has the best catalytic activity when $x = 0.6$ and achieves 90% CO conversion at 163.2°C. In the continuous catalytic oxidation test, $La_{0.4}Sr_{0.6}MnO_3$ can achieve 90% CO catalytic conversion at 176.9°C in the fifth cycle with adequate catalytic stability. Additionally, the effect of water vapor and carbon dioxide on catalytic activity was investigated. The results illustrated that $La_{0.4}Sr_{0.6}MnO_3$ has the highest catalytic activity in the mixture atmosphere and reaches 50% and 90% CO conversion at 153.1°C and 181.5°C. Moreover, in consecutive oxidation experiments, the rapid sintering of precursor sprays in high-temperature flame enhances the dispersion and sintering resistance of Mn active components, thus exhibiting good antisintering properties and superior CO catalytic oxidation performance. The decrease in catalytic activity may be due to the chemisorbed oxygen consumption and the reduction of active sites on the catalyst surface. In conclusion, the flame synthesis is an efficient and convenient method for preparing perovskite catalysts with high CO oxidation activity.

## Data Availability

All data generated or analyzed during this study are included within this article and are available from the corresponding author upon request.

## Conflicts of Interest

The authors declare that they have no conflicts of interest.

## Acknowledgments

This work was supported by National Natural Science Foundation of China (52036008).

## References

[1] I. Manisalidis, E. Stavropoulou, A. Stavropoulos, and E. Bezirtzoglou, "Environmental and health impacts of air pollution: a review," *Frontiers in Public Health*, vol. 8, p. 14, 2020.

[2] S. Li, H. Zhu, Z. Qin et al., "Morphologic effects of nano $CeO_2$-$TiO_2$ on the performance of Au/$CeO_2$-$TiO_2$ catalysts in low-temperature CO oxidation," *Applied Catalysis B: Environmental*, vol. 144, pp. 498–506, 2014.

[3] Y.-G. Chen, Z.-C. Guo, and G.-S. Feng, "NO x reduction by coupling combustion with recycling flue gas in iron ore sintering process," *International Journal of Minerals, Metallurgy, and Materials*, vol. 18, no. 4, pp. 390–396, 2011.

[4] R. Hammami, H. Batis, and C. Minot, "Combined experimental and theoretical investigation of the $CO_2$ adsorption on $LaMnO_3+y$ perovskite oxide," *Surface Science*, vol. 603, no. 20, pp. 3057–3067, 2009.

[5] S. Royer and D. Duprez, "Catalytic oxidation of carbon monoxide over transition metal oxides," *ChemCatChem*, vol. 3, no. 1, pp. 24–65, 2011.

[6] Y. Liu, H. Dai, J. Deng et al., "Mesoporous $Co_3O_4$-supported gold nanocatalysts: highly active for the oxidation of carbon monoxide, benzene, toluene, and o-xylene," *Journal of Catalysis*, vol. 309, pp. 408–418, 2014.

[7] K. Ding, A. Gulec, A. M. Johnson et al., "Identification of active sites in CO oxidation and water-gas shift over supported Pt catalysts," *Science*, vol. 350, no. 6257, pp. 189–192, 2015.

[8] H. Li, K. Yu, C. Wan et al., "Comparison of the nickel addition patterns on the catalytic performances of $LaCoO_3$ for low-temperature CO oxidation," *Catalysis Today*, vol. 281, pp. 534–541, 2017.

[9] E. Frozandeh-Mehr, A. Malekzadeh, M. Ghiasi, A. Gholizadeh, Y. Mortazavi, and A. Khodadadi, "Effect of partial substitution of lanthanum by strontium or bismuth on structural features of the lanthanum manganite nanoparticles as a catalyst for carbon monoxide oxidation," *Catalysis Communications*, vol. 28, pp. 32–37, 2012.

[10] F. Teng, W. Han, S. Liang, B. Gaugeu, R. Zong, and Y. Zhu, "Catalytic behavior of hydrothermally synthesized $La_{0.5}Sr_{0.5}MnO_3$ single-crystal cubes in the oxidation of CO and $CH_4$," *Journal of Catalysis*, vol. 250, no. 1, pp. 1–11, 2007.

[11] P.-Y. Peng, Y.-C. Tsai, J.-T. Yeh, Y.-S. Lin, and C.-M. Huang, "Influence of Sr substitution on catalytic performance of $LaMnO_3$/Ni metal foam composite for CO oxidation," *Aerosol and Air Quality Research*, vol. 15, no. 4, pp. 1662–1671, 2015.

[12] G. Liu, J. Li, K. Yang et al., "Effects of cerium incorporation on the catalytic oxidation of benzene over flame-made perovskite $La_{1-x}Ce_xMnO_3$ catalysts," *Particuology*, vol. 19, pp. 60–68, 2015.

[13] Y. Abe and R. M. Laine, "Photocatalytic $La_4Ti_3O_{12}$ nanoparticles fabricated by liquid-feed flame spray pyrolysis," *Ceramics International*, vol. 46, no. 11, pp. 18656–18660, 2020.

[14] H. Zhou and B. Qi, "Investigation of flame spray synthesized $La_{1-x}Sr_xCoO_3$ perovskites with promotional catalytic performances on CO oxidation," *Journal of the Energy Institute*, vol. 93, no. 6, pp. 2381–2387, 2020.

[15] Y. Abe and R. M. Laine, "Photocatalytic plate-like $La_2Ti_2O_7$ nanoparticles synthesized via liquid-feed flame spray pyrolysis (LF-FSP) of metallo-organic precursors," *Journal of the American Ceramic Society*, vol. 103, no. 9, pp. 4832–4839, 2020.

[16] B.-J. Kim, E. Fabbri, D. F. Abbott et al., "Functional role of Fe-doping in Co-based perovskite oxide catalysts for oxygen evolution reaction," *Journal of the American Chemical Society*, vol. 141, no. 13, pp. 5231–5240, 2019.

[17] W. Haron, A. Wisitsoraat, and S. Wongnawa, "Nanostructured perovskite oxides - $LaMO_3$ (M=Al, Co, Fe) prepared by co-precipitation method and their ethanol-sensing characteristics," *Ceramics International*, vol. 43, no. 6, pp. 5032–5040, 2017.

[18] G. Xu, H. Bai, X. Huang et al., "Self-assembled 3D flower-like perovskite $PbTiO_3$ nanostructures and their application in the catalytic oxidation of CO," *Journal of Materials Chemistry*, vol. 3, no. 2, pp. 547–554, 2015.

[19] S. Wang, X. Xu, J. Zhu, D. Tang, and Z. Zhao, "Effect of preparation method on physicochemical properties and catalytic performances of $LaCoO_3$ perovskite for CO oxidation," *Journal of Rare Earths*, vol. 37, no. 9, pp. 970–977, 2019.

[20] J. A. M. Van Roosmalen, P. Van Vlaanderen, E. H. P. Cordfunke, W. L. Ijdo, and D. J. W. Ijdo, "Phases in the perovskite-type $LaMnO_{3+\delta}$ solid solution and the $La_2O_3$-$Mn_2O_3$ phase diagram," *Journal of Solid State Chemistry*, vol. 114, no. 2, pp. 516–523, 1995.

[21] C. Li, T. Li, B. Wang, and H. Yan, "Synthesis of $La_{1-x}Sr_xMnO_3$ cubic crystals with adjustable doping levels," *Journal of Crystal Growth*, vol. 295, no. 2, pp. 137–140, 2006.

[22] D. V. Ivanov, L. G. Pinaeva, L. A. Isupova, A. N. Nadeev, I. P. Prosvirin, and L. S. Dovlitova, "Insights into the reactivity of $La_{1-x}Sr_xMnO_3$ ($x = 0 \div 0.7$) in high temperature $N_2O$ decomposition," *Catalysis Letters*, vol. 141, no. 2, pp. 322–331, 2010.

[23] C. Zhang, K. Zeng, C. Wang et al., "$LaMnO_3$ perovskites via a facile nickel substitution strategy for boosting propane combustion performance," *Ceramics International*, vol. 46, no. 5, pp. 6652–6662, 2020.

[24] X. Wang, K. Huang, J. Qian, Y. Cong, C. Ge, and S. Feng, "Enhanced CO catalytic oxidation by Sr reconstruction on the surface of La x $Sr_{1-x}CoO_{3-\delta}$," *Science Bulletin*, vol. 62, no. 9, pp. 658–664, 2017.

[25] R. Zhang, A. Villanueva, H. Alamdari, and S. Kaliaguine, "Catalytic reduction of NO by propene over $LaCo_{1-x}Cu_xO_3$ perovskites synthesized by reactive grinding," *Applied Catalysis B: Environmental*, vol. 64, no. 3-4, pp. 220–233, 2006.

[26] C. Zhang, C. Wang, W. Hua et al., "Relationship between catalytic deactivation and physicochemical properties of $LaMnO_3$ perovskite catalyst during catalytic oxidation of vinyl chloride," *Applied Catalysis B: Environmental*, vol. 186, pp. 173–183, 2016.

[27] Q. Gu, L. Wang, Y. Wang, and X. Li, "Effect of praseodymium substitution on $La_{1-x}Pr_xMnO_3$ ($x = 0 - 0.4$) perovskites and catalytic activity for NO oxidation," *Journal of Physics and Chemistry of Solids*, vol. 133, pp. 52–58, 2019.

[28] S. Ding, H.-A. Chen, O. Mekasuwandumrong et al., "High-temperature flame spray pyrolysis induced stabilization of Pt single-atom catalysts," *Applied Catalysis B: Environmental*, vol. 281, 2021.

[29] F. Fang, N. Feng, P. Zhao et al., "In situ exsolution of $Co/CoO_x$ core-shell nanoparticles on double perovskite porous nanotubular webs: a synergistically active catalyst for soot efficient oxidation," *Chemical Engineering Journal*, vol. 372, pp. 752–764, 2019.

[30] J. Sun, Z. Zhao, Y. Li et al., "Synthesis and catalytic performance of macroporous $La_{1-x}Ce_x$ $CoO_3$ perovskite oxide catalysts with high oxygen mobility for catalytic combustion of soot," *Journal of Rare Earths*, vol. 38, no. 6, pp. 584–593, 2020.

[31] B. Kucharczyk, "Catalytic oxidation of carbon monoxide on Pd-containing $LaMnO_3$ perovskites," *Catalysis Letters*, vol. 145, no. 6, pp. 1237–1245, 2015.

[32] X. Yuan, M. Qing, L. Meng, and H. Zhao, "One-step synthesis of nanostructured Cu-Mn/$TiO_2$ via flame spray pyrolysis: application to catalytic combustion of CO and $CH_4$," *Energy & Fuels*, vol. 34, no. 11, pp. 14447–14457, 2020.